

Robust Majorana signature detection with a coupled quantum dot-nanomechanical resonator in all-optical domain

¹Hua-Jun Chen[†], ¹Chang-Zhao Chen, ¹Xian-Wen Fang, ¹Yang

Li, ¹Guang-Hong Miao, ²Shao-Fei Tu, and ²Ka-Di Zhu*

¹*School of Science, Anhui University of Science and Technology,*

Huainan Anhui, 232001, China and

²*Key Laboratory of Artificial Structures and Quantum Control (Ministry of Education),*

Department of Physics and Astronomy, Shanghai Jiao Tong University,

800 DongChuan Road, Shanghai 200240, China

Abstract

Motivated by a recent experiment [Nadj-Perge et al., Science 346, 602 (2014)] providing evidence for Majorana zero modes in iron chains on the superconducting Pb surface, in the present work, we theoretically propose an all-optical scheme to detect Majorana fermions, which is very different from the current tunneling measurement based on electrical means. The optical detection proposal consists of a quantum dot embedded in a nanomechanical resonator with optical pump-probe technology. With the optical means, the signal in the coherent optical spectrum presents a distinct signature for the existence of Majorana fermions in the end of iron chains. Further, the vibration of the nanomechanical resonator behaving as a phonon cavity will enhance the exciton resonance spectrum, which makes the Majorana fermions more sensitive to be detectable. This optical scheme affords a potential supplement for detection of Majorana fermions and supports to use Majorana fermions in Fe chains as qubits for potential applications in quantum computing devices.

PACS numbers: 73.21.-b, 63.22.-m, 42.50.-p, 78.67.Hc

INTRODUCTION

Majorana fermions (MFs) are real solutions of the Dirac equation and which are their own antiparticles $\gamma = \gamma^\dagger$ [1]. Although proposed originally as a model for neutrinos, MFs have recently been predicted to occur as quasi-particle bound states in engineered condensed matter systems [2]. This exotic particle obeys non-Abelian statistics, which is one of important factors to realize subsequent potential applications in decoherence-free quantum computation [3–5] and quantum information processing [6, 7]. Over the recent few years, the possibility for hosting MFs in exotic solid state systems focused on topological superconductors [2, 3, 7]. Currently, various realistic platforms including topological insulators [8, 9], semiconductor nanowires (SNWs) [10, 11], and atomic chains [12–15] have been proposed to support Majorana states based on the superconducting proximity effect. Although various schemes have been presented, observing the unique Majorana signatures experimentally is still a challenging task to conquer.

MFs are their own antiparticles, and they are predicted to appear in tunneling spectroscopy experiments, in which Majoranas manifest themselves as characteristic zero-bias peaks (ZBPs) [16, 17]. The theoretical predictions of ZBPs have been observed experimentally in SNWs which are interpreted as the signatures of MFs [18–22]. Remarkably, Nadj-Perge et al. [23] recently designed a chain of magnetic Fe atoms deposited on the surface of an s-wave superconducting Pb with strong spin-orbit interactions, and reported the striking observation of a ZBP at the end of the atomic chains with STM, which provides evidence for Majorana zero modes. However, these above experimental results can not serve as definitive evidences to prove the existence of MFs in condensed matter systems, and it is also a major challenge in these experiments to uniquely distinguish Majoranas from conventional fermionic subgap states. The first reason is that the zero-bias conductance peaks can also appear in terms of the other mechanisms [24, 25], such as the zero-bias anomaly due to Kondo resonance [22, 26] and the disorder or band bending in the SNW [27]. The second one is that Andreev bound states in a magnetic field can also exhibit a zero-energy crossing as a function of exchange interaction or Zeeman energy [28, 29], and therefore give rise to similar conductance features. As far as we know, most of the experimental evidences for Majorana bound states largely relies on measurements of the tunneling conductance at present, and the observation of Majorana signature based on electrical methods still remains

a subject of debate. Identifying MFs only through tunnel spectroscopy is somewhat problematic. Therefore, to obtain definitive signatures of MFs, alternative setups or proposals for detecting MFs are necessary. Here, we will propose an alternative all-optical scheme to detect MFs.

Benefitting from recent advances in nanotechnology and nanofabrication, nanostructures such as quantum dots (QDs) and nanomechanical resonators (NRs) have been obtained significant progress in modern nanoscience and nanotechnology. QD, as a simple stationary atom with well optical property [30], lays the foundation for numerous possible applications [31]. Due to high natural frequencies and large quality factors of NRs [32], if QDs coupled to NRs [33–35] to form hybrid systems, the coherent optical properties will be enhanced remarkably, which will be an alternative ultrasensitive detection means. Although probing MFs with QDs [36–40] have been proposed, we notice that all the schemes are still based on electrical means. In the present work, we propose an optical measurement scheme to detect the existence of MFs in iron chains on the superconducting Pb surface [23] via a coupled hybrid QD-NR system with optical pump-probe scheme [41].

Compared with electrical detection means where the QDs are coupled to MFs via the tunneling [36–40], in our optical scheme, there is no direct contact between MFs and the hybrid QD-NR system, which can effectively avoid introducing other signals disturbing the detecting of MFs. The interaction between MFs in iron chains and QD in hybrid QD-NR system is mainly due to the dipole-dipole interaction, and the distance between the two systems can be adjusted by several tens of nanometers, therefore the tunneling between the QD and MFs can be neglected safely. In addition, the QD is considered as a two-level system rather than a single resonant level with spin-singlet state, and once MFs appear in the end of iron chains and couple to the QD, the Majorana signature will be carried out via the coherent optical spectrum of the QD. The change in the coherent optical spectrum as a possible signature for MFs is another potential evidence in the iron chains. This optical scheme will provide another method for the detection of MFs, which is very different from the zero-bias peak in the tunneling experiments [18–23]. Furthermore, in order to investigate the role of the NR in the hybrid system, we further introduce the exciton resonance spectrum to detect MFs. The results shows that the vibration of the NR acting as a phonon cavity will enhance the exciton resonance spectrum significantly and make MFs more sensitive to be detectable. The technique proposed here provide a new platform for applications ranging

from robust manipulation of MFs and MFs based quantum information processing.

MODEL AND THEORY

Figure 1(b) shows the schematic setup that will be studied in this work, where iron (Fe) chains on the superconducting Pb(110) surface [23], and we employ a two-level QD with optical pump-probe technology to detect MFs. The Fe chain is ferromagnetically ordered [23] with a large magnetic moment, which takes the role of the magnetic field in the nanowire experiments [18]. Different from the proposal of Mourik et al. [18], this "magnetic field" is mostly localized on the Fe chain, with small leakage outside, and superconductivity is not destroyed along the chain. In this setup, the energy scale of the exchange coupling of the Fe atoms is typically much larger than that of the Rashba spin-orbit coupling and the superconducting pairing. Figure 1(c) displays that a QD is implanted in the NR to form a coupled hybrid QD-NR system. The whole system includes two kinds of couplings which are QD-MF coupling and QD-NR coupling as shown in Fig. 1(a). In the following, we will discuss the two kinds of coupling in detail, respectively.

In the hybrid QD-NR system, the QD is modeled as a two-level system consisting of the ground state $|g\rangle$ and the single exciton state $|e\rangle$ at low temperatures [42, 43], and the Hamiltonian of the QD can be described as $H_{QD} = \hbar\omega_e S^z$ with the exciton frequency ω_e , where S^z and S^\pm are the pseudospin operator describing the two-level exciton with the commutation relation $[S^z, S^\pm] = \pm S^\pm$ and $[S^+, S^-] = 2S^z$. For the NR, the thickness of the beam is much smaller than its width, the lowest-energy resonance corresponds to the fundamental flexural mode that will constitute the resonator mode [33] which can be characterized by a quantum harmonic oscillator with Hamiltonian $H_{NR} = \hbar\omega_n(b^\dagger b + 1/2)$, where ω_n is the resonator frequency and b is the annihilation operator of the resonator mode. Since the flexion induces extensions and compressions in the structure [44], this longitudinal strain will modify the energy of the electronic states of QD through deformation potential coupling. Then the coupling between the resonator mode and the QD is described by $H_{int} = \hbar\omega_n g S^z (b^\dagger + b)$, where g is the coupling strength between the resonator mode and QD [33]. Thus we obtain the Hamiltonian of the coupled hybrid QD-NR system

$$H_{QD-NR} = \hbar\omega_e S^z + \hbar\omega_n (b^\dagger b + 1/2) + \hbar\omega_n g S^z (b^\dagger + b). \quad (1)$$

For the QD-MF coupling, as each MF is its own antiparticle, we introduce an operator γ with $\gamma^\dagger = \gamma$ and $\gamma^2 = 1$ to describe MFs. Supposed that the QD couples to the nearby MF γ_1 in the end of iron chains, then the Hamiltonian is written by [36–40]

$$H = i\epsilon_M\gamma_1\gamma_2/2 + i\hbar\beta(S^- - S^+)\gamma_1. \quad (2)$$

To detect MFs, it is helpful to switch the Majorana representation to the regular fermion one via the exact transformation $\gamma_1 = f^\dagger + f$ and $\gamma_2 = i(f^\dagger - f)$, where f and f^\dagger are the fermion annihilation and creation operators obeying the anti-commutative relation $\{f, f^\dagger\} = 1$. Accordingly, in the rotating wave approximation [45], the above Hamiltonian can be rewritten as

$$H_{MF-QD} = \epsilon_M(f^\dagger f - 1/2) + i\hbar\beta(S^- f^\dagger - S^+ f), \quad (3)$$

where the first term gives the energy of MF with frequency ω_M and $\epsilon_M = \hbar\omega_M \sim e^{-l/\xi}$ with the iron chains length (l) and the Pb superconducting coherent length (ξ). If the iron chains length (l) is large enough, ϵ_M will approach zero. In the following, we will discuss the two conditions of $\epsilon_M \neq 0$ and $\epsilon_M = 0$, and define the two conditions as coupled MFs ($\epsilon_M \neq 0$) and uncoupled MFs ($\epsilon_M = 0$), respectively. The second term describes the coupling between the nearby MF and the QD with the coupling strength β , where the coupling strength is related to the distance between the hybrid QD-NR system and the iron chains. It should be also noted that the term of non-conservation for energy, i.e. $i\hbar\beta(S^- f - S^+ f^\dagger)$, is generally neglected. We have made the numerical calculations (not shown in the following figures) and shown that the effect of this term is too small to be considered in our theoretical treatment.

Currently, the optical pump-probe technique has become a popular topic, which affords an effective way to investigate the light-matter interaction. The optical pump-probe technology includes a strong pump laser and a weak probe laser [46]. In the optical pump-probe technology, the strong pump laser is used to stimulate the system to generate coherent optical effect, while the weak laser plays the role of probe laser. Therefore, the linear and nonlinear optical effects can be observed via the probe absorption spectrum based on the optical pump-probe scheme. Xu et al. have obtained coherent optical spectroscopy of semiconductor QD when driven simultaneously by two optical fields [41]. Their results open the way for the demonstration of numerous quantum level-based applications, such as QD lasers, optical modulators, and quantum logic devices. In terms of this scheme, we apply the pump-probe scheme to the QD of the hybrid QD-NR system simultaneously. When the

optical pump-probe technology is applied on the QD, the Majorana signature will be carried out via the coherent optical spectrum. The Hamiltonian of the exciton of the QD coupled to the two fields is given by [46] $H_{P-QD} = -\mu \sum_{k=pu,pr} E_k (S^+ e^{-i\omega_k t} + S^- e^{i\omega_k t})$, where μ is the dipole moment of the exciton, and E_k is the slowly varying envelope of the field.

Therefore, we obtain the whole Hamiltonian of the hybrid system as $H = H_{QD-NR} + H_{MF-QD} + H_{P-QD}$. In a rotating frame at the pump field frequency ω_{pu} , we obtain the total Hamiltonian of the system as

$$H = \hbar\Delta_{pu}S^z + \hbar\omega_n(b^+b + 1/2) + \hbar\omega_ngS^z(b^+ + b) + \hbar\Delta_M(f^\dagger f - 1/2) + i\hbar\beta(S^- f^\dagger - S^+ f) - \hbar\Omega_{pu}(S^+ + S^-) - \mu E_{pr}(S^+ e^{-i\delta t} + S^- e^{i\delta t}), \quad (4)$$

where $\Delta_{pu} = \omega_e - \omega_{pu}$ is the detuning of the exciton frequency and the pump frequency, $\Omega_{pu} = \mu E_{pu}/\hbar$ is the Rabi frequency of the pump field, and $\delta = \omega_{pr} - \omega_{pu}$ is the detuning of the probe field and the pump field. $\Delta_M = \omega_M - \omega_{pu}$ is the detuning of the MF frequency and the pump frequency. Actually, we have neglected the regular fermion like normal electrons in the nanowire that interact with the QD in the above discussion. To describe the interaction between the normal electrons and the exciton in QD, a tight binding Hamiltonian of the whole iron chains is introduced [47].

According to the Heisenberg equation of motion and introducing the corresponding damping and noise terms, the quantum Langevin equations of the whole system are derived as

$$\dot{S}^z = -\Gamma_1(S^z + 1/2) - \beta(S^- f^\dagger + S^+ f) + i\Omega_{pu}(S^+ - S^-) + \frac{i\mu E_{pr}}{\hbar}(S^+ e^{-i\delta t} - S^- e^{i\delta t}), \quad (5)$$

$$\dot{S}^- = -[i(\Delta_{pu} + \omega_n g Q) + \Gamma_2]S^- + 2(\beta f - i\Omega_{pu})S^z - \frac{2i\mu E_{pr}}{\hbar}e^{-i\delta t}S^z + \hat{\tau}(t), \quad (6)$$

$$\dot{f} = -(i\Delta_M + \kappa_M/2)f + \beta S^- + \hat{\zeta}(t), \quad (7)$$

$$\ddot{Q} + \gamma_n \dot{Q} + \omega_n^2 Q = -2\omega_n^2 g S^z + \hat{\xi}(t), \quad (8)$$

where Γ_1 (Γ_2) is the exciton spontaneous emission rate (dephasing rate), $Q = b^+ + b$ is the position operator, γ_n is the decay rate of the NR, and κ_M is the decay rate of the MF. $\hat{\tau}(t)$ is the δ -correlated Langevin noise operator, which has zero mean $\langle \hat{\tau}(t) \rangle = 0$ and obeys the correlation function $\langle \hat{\tau}(t) \hat{\tau}^\dagger(t') \rangle \simeq \delta(t - t')$. The resonator mode is affected by a Brownian stochastic force with zero mean value, and $\hat{\xi}(t)$ has the correlation function

$$\langle \hat{\xi}^+(t) \hat{\xi}(t') \rangle = \frac{\gamma_n}{\omega_n} \int \frac{d\omega}{2\pi} \omega e^{-i\omega(t-t')} [1 + \coth(\hbar\omega/2\kappa_B T)], \quad (9)$$

where k_B and T are the Boltzmann constant and the temperature of the reservoir of the coupled system. MFs have the same correlation relation as the resonator mode as

$$\langle \hat{\varsigma}^+(t)\hat{\varsigma}(t') \rangle = \frac{\kappa_M}{\omega_M} \int \frac{d\omega}{2\pi} \omega e^{-i\omega(t-t')} [1 + \coth(\hbar\omega/2\kappa_B T)]. \quad (10)$$

In Eq.(9) and Eq.(10), both the NR and Majorana mode will be affected by a thermal bath of Brownian and non-Markovian processes [48]. In the low temperature, the quantum effects of both the Majorana and NR mode are only observed in the case of $\omega_M/\kappa_M \gg 1$ and $\omega_n/\gamma_n \gg 1$. Due to the weak coupling to the thermal bath, the Brownian noise operator can be modeled as Markovian processes. In addition, both the QD-MFs coupling and QD-NR mode coupling in the hybrid system are stronger than the coupling to the reservoir that influences the two kinds coupling. In this case, owing to the second order approximation [48], we can obtain the form of the reservoir that affects both the NR mode and Majorana mode as Eq.(9) and Eq.(10).

To go beyond weak coupling, the Heisenberg operator can be rewritten as the sum of its steady-state mean value and a small fluctuation with zero mean value

$$S^z = S_0^z + \delta S^z, S^- = S_0^- + \delta S^-, f = f_0 + \delta f, Q = Q_0 + \delta Q \quad (11)$$

Since the driving fields are weak, but classical coherent fields, we will identify all operators with their expectation values, and drop the quantum and thermal noise terms. Simultaneously, inserting these operators into the Langevin equations Eqs.(5)-(8) and neglecting the nonlinear term, we can obtain two equation sets about the steady-state mean value and the small fluctuation. The steady-state equation set consisting of f_0 , Q_0 and S_0 is related to the population inversion ($w_0 = 2S_0^z$) of the exciton which is determined by

$$\begin{aligned} & \Gamma_1(w_0 + 1)[(\Delta_M^2 + \kappa_M^2/4)(\Delta_{pu}^2 + \Gamma_2^2 + \omega_n^2 g^4 w_0^2 - 2\omega_n \Delta_{pu} g^2 w_0) \\ & + \beta^2 w_0^2 (\beta^2 - 2\omega_n \Delta_M g^2 + 2\Delta_{pu} \Delta_M - \Gamma_2 \kappa_M)] + 4w_0 \Gamma_2 \Omega_{pu}^2 (\Delta_M^2 + \kappa_M^2/4) = 0. \end{aligned} \quad (12)$$

For the equation set of small fluctuation, we make the ansatz [46] $\langle \delta O \rangle = O_+ e^{-i\delta t} + O_- e^{i\delta t}$ ($O = S^z, S^-, f, Q$). Solving the equation set and working to the lowest order in E_{pr} but to all orders in E_{pu} , we can obtain the linear susceptibility as $\chi_{eff}^{(1)}(\omega_{pr}) = \mu S_+(\omega_{pr})/E_{pr} = (\mu^2/\hbar\Gamma_2)\chi^{(1)}(\omega_{pr})$, where $\chi^{(1)}(\omega_{pr})$ is given by

$$\chi^{(1)}(\omega_{pr}) = \frac{[(\Pi_4^* + \Lambda_1 \Pi_3^*)\Pi_1 \Lambda_3 - i w_0 \Pi_4^*] \Gamma_2}{\Pi_2 \Pi_4^* - \Lambda_1 \Lambda_2 \Pi_1 \Pi_3^*}, \quad (13)$$

f_0 , S_0 and Q_0 can be derived from the steady-state equations, and $\Sigma_1 = \beta/(i\Delta_M + \kappa_M/2 - i\delta)$, $\Sigma_2 = \beta/(-i\Delta_M + \kappa_M/2 - i\delta)$, $\eta = 2g\omega_n^2/(\delta^2 + i\delta\gamma_n - \omega_n^2)$, $\Lambda_1 = [i\Omega_{pu} - \beta(f_0 + S_0\Sigma_2^*)]/(\Gamma_1 - i\delta)$, $\Lambda_2 = [-i\Omega_{pu} - \beta(f_0^* + S_0^*\Sigma_1)]/(\Gamma_1 - i\delta)$, $\Lambda_3 = iS_0^*/(\Gamma_1 - i\delta)$, $\Pi_1 = 2(\beta f_0 - i\Omega_{pu}) - i\omega_n g S_0 \eta$, $\Pi_2 = i(\Delta_{pu} - \delta + \omega_n g Q_0) + \Gamma_2 - \beta w_0 \Sigma_1 - \Lambda_2 \Pi_1$, $\Pi_3 = 2(g f_0 - i\Omega_{pu}) - i\omega_n g S_0 \eta^*$, $\Pi_4 = i(\Delta_{pu} + \delta + \omega_n g Q_0) + \Gamma_2 - \beta w_0 \Sigma_2 - \Lambda_3 \Pi_3$ (\Re^* indicates the conjugate of \Re). The imaginary and real parts of $\chi^{(1)}(\omega_{pr})$ indicate absorption and dissipation, respectively. In addition, the average population of the exciton states can be obtained as

$$S_+^z = \frac{(\Lambda_1 \Pi_3^* + \Pi_4^*)[\Lambda_3(\Pi_2 + \Lambda_2 \Pi_1) - i w_0 \Lambda_2]}{\Pi_2 \Pi_4^* - \Lambda_1 \Lambda_2 \Pi_1 \Pi_3^*}, \quad (14)$$

which is benefited for readout the exciton states of QD.

NUMERICAL RESULTS AND DISCUSSIONS

For illustration of the numerical results, we choose the realistic hybrid systems of the coupled QD-NR system [33] and the iron chains on the superconducting Pb surface [23]. For an InAs QD in the coupled QD-NR system, we use parameters [33]: the exciton relaxation rate $\Gamma_1 = 0.3$ GHz, the exciton dephasing rate $\Gamma_2 = 0.15$ GHz. The physical parameters of GaAs NR are $(\omega_n, M, Q_f) = (1.2 \text{ GHz}, 5.3 \times 10^{-18} \text{ kg}, 3 \times 10^4)$, where ω_n , M , and Q_f are the resonator frequency, the effective mass, and quality factor of the NR, respectively. The decay rate of the NR is $\gamma_n = \omega_n/Q_f = 40$ kHz, and the coupling strength between the QD and NR is $g = 0.06$. For MFs, there are no experimental values for the lifetime of the MFs and the coupling strength between the exciton and MFs in the recent literature. However, according to a few recent experimental reports [18–23], it is reasonable to assume that the lifetime of the MFs is $\kappa_M = 0.1$ MHz. Since the coupling strength between the QD and nearby MFs is dependent on their distance, we also expect the coupling strength $\beta = 0.05$ GHz via adjusting the distance between the hybrid QD-NR system and the iron chains.

Figure 2(a) shows the coherent optical properties of the QD as functions of probe-exciton detuning $\Delta_{pr} = \omega_{pr} - \omega_e$ at the detuning of the exciton frequency and the pump frequency $\Delta_{pu} = 0$, i.e., the absorption ($Im\chi^{(1)}$) and dissipation ($Re\chi^{(1)}$) properties of the QD without considering any coupling ($g = 0, \beta = 0$), which indicates the normal absorption and dissipation of the QD, respectively. Turning on the QD-NR coupling ($g = 0.06$) and without considering the QD-MF coupling ($\beta = 0$), two sharp peaks will appear in both the absorp-

tion and dissipation spectra as shown in Fig. 2(b). From the curves, we find that the two sharp peaks at both sides of the spectra just correspond to the vibrational frequency of the NR. The physical origin of this result is due to mechanically induced coherent population oscillation, which makes quantum interference between the resonator and the beat of the two optical fields via the QD when the probe-pump detuning is equal to the NR frequency [49]. This reveals that if fixing the pump field on-resonance with the exciton and scan through the frequency spectrum, the two sharp peaks can obtain immediately in the coherent optical spectra, which also indicates a scheme to measure the frequency of the NR. This phenomenon stems from the quantum interference between the vibration NR and the beat of the two optical fields via the exciton when probe-pump detuning δ is adjusted equal to the frequency of the NR. Therefore, the QD-NR coupling play a key role in the hybrid system, and if we ignore the coupling ($g = 0$), the above phenomenon will disappear completely as shown in Fig. 2(a).

Compared with Fig.2(b), in Fig.2(c), we consider the QD coupled with the nearby MF γ_1 without taking the QD-NR coupling into account, i.e. the condition of $g = 0$ and $\beta = 0.05$ GHz. As the MFs appear in the ends of iron chains and coupled to the QD, both the probe absorption (the blue curve) and dissipation (the green curve) spectra will present an remarkable signature of MFs under $\Delta_M = -0.5$ GHz. The physical origin of this result is due to the QD-MF coherent interaction and we can interpret this physical phenomenon with dressed state between the exciton and MFs. The QD coupled to the nearby MF will induce the upper level of the state $|e\rangle$ to split into $|e, n_M\rangle$ and $|e, n_M + 1\rangle$ (n_M denotes the number states of the MFs). The left peak in the coherent optical spectra signifies the transition from $|g\rangle$ to $|e, n_M\rangle$ while the right peak is due to the transition of $|g\rangle$ to $|e, n_M + 1\rangle$ [47]. To determine this signature is the true MFs rather than the normal electrons that couple with the QD, we have used a tight binding Hamiltonian to describe the electrons in whole iron chains, the numerical results indicate the signals in the absorption and dissipation spectra are the true MFs signature [50]. If we consider both the two kinds coupling, i.e. the QD-NR coupling ($g = 0.06$) and QD-MFs coupling ($\beta = 0.05$ GHz) as shown in Fig. 2(d), not only the two sharp peaks locate at the NR frequency induced by its vibration, i.e. two peaks are at $\Delta_{pr} = \pm 1.2$ GHz ($\omega_n = 1.2$ GHz), there is also MFs signal appear at $\Delta_{pr} = -0.5$ GHz ($\Delta_M = -0.5$ GHz) induced by the QD-MF coupling.

In Fig. 2(c), we only consider the situation of $\epsilon_M \neq 0$. In fact, if the iron chains length

l is much larger than the Pb superconducting coherent length ξ , ϵ_M will approach zero. Therefore, it is necessary to consider the conditions of $\epsilon_M \neq 0$ and $\epsilon_M = 0$, and we define them as coupled MFs mode ($\epsilon_M \neq 0$) and uncoupled MFs mode ($\epsilon_M = 0$), respectively. Figure 3(a) and Figure 3(b) show the absorption and dissipation spectra as a function of detuning Δ_{pr} with QD-MF coupling constants $\beta = 0.05$ GHz under $\epsilon_M \neq 0$ and $\epsilon_M = 0$, respectively. Compared with the coupled MFs mode, the uncoupled QD-MF Hamiltonian will reduce to $H_{MF-QD} = i\hbar\beta(S^-f^\dagger - S^+f)$ which is analogous J-C Hamiltonian of standard model under $\epsilon_M = 0$, and the probe absorption spectrum (the blue curve) shows a symmetric splitting as the QD-MF coupling strength $\beta = 0.05$ GHz which is different from of coupled MFs mode presenting unsymmetric splitting due to a detuning $\Delta_M = -0.5$ GHz. Therefore, our results reveal that the signals in the coherent optical spectra is a real signature of MF, and the optical detection scheme can work at both the coupled Majorana edge states and the uncoupled Majorana edge states.

In Fig. 3(c), we further make a comparison of the probe absorption spectrum under the coupled MFs mode ($\epsilon_M \neq 0$) and uncoupled MFs mode ($\epsilon_M = 0$). It is obvious that the probe absorption spectrum display the analogous phenomenon of electromagnetically induced transparency (EIT) [51] under both the two conditions. The dip in the probe absorption spectrum goes to zero at $\Delta_{pr} = 0$ and $\Delta_{pr} = -0.5$ GHz with $\epsilon_M = 0$ and $\epsilon_M \neq 0$, respectively, which means the input probe field is transmitted to the coupled system without absorption. Such a phenomenon is attributed to the destructive quantum interference effect between the Majorana modes and the beat of the two optical fields via the QD. If the beat frequency of two lasers δ is close to the resonance frequency of MFs, the Majorana mode starts to oscillate coherently, which results in Stokes-like ($\Delta_S = \omega_{pu} - \omega_M$) and anti-Stokes-like ($\Delta_{AS} = \omega_{pu} + \omega_M$) scattering of light from the QD. The Stokes-like scattering is strongly suppressed because it is highly off-resonant with the exciton frequency. However, the anti-Stokes-like field can interfere with the near-resonant probe field and thus modify the probe field spectrum. Here the Majorana modes play a vital role in this coupled system, and we can refer the above phenomenon as Majorana modes induced transparency, which is analogous with EIT in atomic systems [51].

On the other hand, we can propose a means to determine the QD-MF coupling strength β via measuring the distance of the two peaks with increasing the QD-MF coupling strength in the probe absorption spectrum. Figure 3(d) indicates the peak-splitting width as a

function of the QD-MF coupling strength β under the condition of the coupled MFs mode ($\epsilon_M \neq 0$) and the uncoupled MFs mode ($\epsilon_M = 0$) which follows a nearly linear relationship. It is obvious that the two lines (the uncoupled MFs and the coupled MFs mode) have a slight deviation. However, the deviation becomes slighter with increasing coupling strength. Therefore, it is essential to enhance the coupling strength for a clear peak splitting via adjusting the distance between the QD and the nearby MFs. In this case the coupling strength can obtain immediately by directly measuring the distance of the two peaks in the probe absorption spectrum.

As shown in Fig. 2(d), there are not only two sharp peaks locate at the NR frequency induced by its vibration but also the MFs signal appear at $\Delta_{pr} = \Delta_M$ induced by the QD-MF coupling in the probe absorption spectrum (the blue curve) under the two kinds coupling. In Fig. 4(a), we further consider switching the detuning $\Delta_M = -0.5$ GHz to $\Delta_M = -1.2$ GHz at small exciton-pump detuning $\Delta_{pu} = 0.05$ GHz. It is obvious that the resonance amplification process (1) and the resonance absorption process (2) in the probe absorption spectrum without considering the QD-MF coupling (the blue curve, $\beta = 0$) will accordingly transform into the the resonance absorption process (3) and the resonance amplification process (4) due to the QD-MF coupling (the green curve, $\beta = 0.1$ GHz). Return to Fig. 1(a), there are two kinds of coupling which are QD-NR coupling and QD-MF coupling in the hybrid system. For the QD-NR system, the two sharp peaks in the probe absorption corresponding to the resonance amplification (1) and absorption process (2) can be elaborated with dressed states $|g, n\rangle$, $|g, n+1\rangle$, $|e, n\rangle$, $|e, n+1\rangle$ ($|n\rangle$ denotes the number state of the resonance mode), and the two sharp peaks indicate the transition between the dressed states [49]. However, once MFs appear in the ends of iron chains and coupled to the QD, the ground state $|g\rangle$ and the exciton state $|e\rangle$ of the QD will also modify by the number states of the MFs n_M and induce the Majorana dressed states $|g, n_M\rangle$, $|g, n_M+1\rangle$, $|e, n_M\rangle$, $|e, n_M+1\rangle$. With increasing the QD-MF coupling, the Majorana dressed states will affect the amplification (1) and absorption process (2) significantly, and even realize the inversion between the absorption (3) and amplification (4) process due to the QD-MF coherent interaction (the green curve).

To illustrate the advantage of the NR in the hybrid system, we introduce the exciton resonance spectrum to investigate the role of NR in the coupled QD-NR, which is benefited for readout the exciton states of QD. In Fig. 4(b), we adjust the detuning $\Delta_M = -0.5$

GHz to $\Delta_M = -1.2$ GHz, therefore, the location of the two sideband peaks induced by the QD-MF coupling coincides with the two sharp peaks induced by the vibration of NR, thus the NR is resonant with the coupled QD-MF system and makes the coherent interaction of QD-MF more strong. Figure 4(b) shows the exciton resonance spectrum of the probe field as a function of the probe detuning Δ_{pr} with the detuning $\Delta_{pu} = 0.05$ GHz under the coupled MFs mode $\epsilon_M \neq 0$. The black and red curves correspond to $g = 0$ and $g = 0.06$ for the QD-MF coupling $\beta = 0.1$ GHz, respectively. It is obvious that the role of NR is to narrow and to increase the exciton resonance spectrum. In this case, the NR behaves as a phonon cavity will enhance the sensitivity for detecting MFs.

CONCLUSION

We have proposed an all-optical means to detect the existence of MFs in iron chains on the superconducting Pb surface with a hybrid QD-NR system. The signals in the coherent optical spectra indicate the possible Majorana signature, which provides another supplement for detecting MFs. Due to the vibration of NR, the exciton resonance spectrum becomes much more significant and then enhances the detection sensitivity of MFs. In addition, the QD-MF coupling in our system is a little feeble, while Ref. [35] presents a strong QD-MF coupling and the coupling strength can reach kilohertz, which is beneficial for MFs detection. On the other hand, if we consider embedding a metal nanoparticle-quantum dot (MNP-QD) complex [47, 49] in the NR, the surface plasmon induced by the MNP will enhance the coherent optical property of QD, which may be robust for probing MFs. The concept proposed here, based on the quantum interference between the NR and the beat of the two optical fields, is the first all-optical means to probe MFs. This coupled system will provide a platform for applications in all-optically controlled topological quantum computing based on MFs.

ACKNOWLEDGMENTS

The authors gratefully acknowledge support from the National Natural Science Foundation of China (No.11574206, No.10974133, No.11274230, No.61272153, No.61572035, No.51502005, and No.11404005), the Key Foundation for Young Talents in College of An-

hui Province (NO. 2013SQRL026ZD), and the Foundation for PhD in Anhui University of Science and Technology.

* Electronic address: chenphysics@126.com

- [1] E. Majorana, *Nuovo Cimento* **14**, 171 (1937).
- [2] J. Alicea, *Rep. Prog. Phys.* **75**, 076501 (2012).
- [3] C. W. J. Beenakker, *Annu. Rev. Condens. Matter Phys.* **4**, 113 (2013).
- [4] T. D. Stanescu and S. Tewari, *J. Phys. Condens. Matter* **25**, 233201 (2013).
- [5] M. Franz, *Nat. Nanotechnol.* **8**, 149 (2013).
- [6] C. Nayak, S. H. Simon, A. Stern, M. Freedman, and S. D. Sarma, *Rev. Mod. Phys.* **80**, 1083 (2008).
- [7] S. R. Elliott and M. Franz, *Rev. Mod. Phys.* **87**, 137 (2015).
- [8] L. Fu and C. L. Kane, *Phys. Rev. Lett.* **100**, 096407 (2008).
- [9] L. Fu and C. L. Kane, *Phys. Rev. B* **79**, 161408(R) (2009).
- [10] R. M. Lutchyn, J. D. Sau, and S. Das Sarma, *Phys. Rev. Lett.* **105**, 077001 (2010).
- [11] Y. Oreg, G. Refael, and F. von Oppen, *Phys. Rev. Lett.* **105**, 177002 (2010).
- [12] S. Nadj-Perge, I. K. Drozdov, B. A. Bernevig, and A. Yazdani, *Phys. Rev. B* **88**, 020407(R) (2013).
- [13] M. M. Vazifeh and M. Franz, *Phys. Rev. Lett.* **111**, 206802 (2013).
- [14] Y. Kim, M. Cheng, B. Bauer, R. M. Lutchyn, and S. Das Sarma, *Phys. Rev. B* **90**, 060401(R) (2014).
- [15] Y. Peng, F. Pientka, L. I. Glazman, and F. von Oppen, *Phys. Rev. Lett.* **114**, 106801 (2015).
- [16] K. T. Law, P. A. Lee, and T. K. Ng, *Phys. Rev. Lett.* **103**, 237001 (2009).
- [17] K. Flensberg, *Phys. Rev. B* **82**, 180516 (2010).
- [18] V. Mourik, K. Zuo, S. M. Frolov, S. R. Plissard, E. P. A. M. Bakkers, and L. P. Kouwenhoven, *Science* **336**, 1003 (2012).
- [19] A. Das, Y. Ronen, Y. Most, Y. Oreg, M. Heiblum, and H. Shtrikman, *Nat. Phys.* **8**, 887 (2012).
- [20] M. T. Deng, C. L. Yu, G. Y. Huang, M. Larsson, P. Caroff, and H. Q. Xu, *Nano Lett.* **12**, 6414 (2012).

- [21] H. O. H. Churchill, V. Fatemi, K. Grove-Rasmussen, M. T. Deng, P. Caroff, H. Q. Xu, and C. M. Marcus, Phys. Rev. B **87**, 241401(R) (2013).
- [22] A. D. K. Finck, D. J. Van Harlingen, P. K. Mohseni, K. Jung, and X. Li, Phys. Rev. Lett. **110**, 126406 (2013).
- [23] S. Nadj-Perge, I. K. Drozdov, J. Li, H. Chen, S. Jeon, J. Seo, A. H. MacDonald, B. A. Bernevig, A. Yazdani, Science **346**, 602 (2014).
- [24] J. Liu, A. C. Potter, K. T. Law, and P. A. Lee, Phys. Rev. Lett. **109**, 267002 (2012).
- [25] W. Chang, V. E. Manucharyan, T. S. Jespersen, J. Nygard, and C. M. Marcus, Phys. Rev. Lett. **110**, 217005 (2013).
- [26] E. J. H. Lee, X. Jiang, R. Aguado, G. Katsaros, C. M. Lieber, and S. De Franceschi, Phys. Rev. Lett. **109**, 186802 (2012).
- [27] D. Bagrets and A. Altland, Phys. Rev. Lett. **109**, 227005 (2012).
- [28] K. J. Franke, G. Schulze, and J. I. Pascual, Science **332**, 940 (2011).
- [29] E. J. H. Lee, X. Jiang, M. Houzet, R. Aguado, C. M. Lieber, and S. D. Franceschi, Nat. Nanotechnol. **9**, 79 (2014).
- [30] G. Jundt, L. Robledo, A. Högele, S. Fält, A. Imamöglu, Phys. Rev. Lett. **100**, 177401 (2008).
- [31] B. Urbaszek, X. Marie, T. Amand, O. Krebs, P. Voisin, P. Maletinsky, A. Högele, and A. Imamoglu, Rev. Mod. Phys. **85**, 79 (2013).
- [32] M. Poot, H. S. J. van der Zant, Phys. Rep. **511**, 273 (2013).
- [33] I. Wilson-Rae, P. Zoller, and A. Imamoglu, Phys. Rev. Lett. **92**, 075507 (2004).
- [34] I. Yeo, P. L. de Assis, A. Gloppe, E. Dupont-Ferrier, P. Verlot, N. S. Malik, E. Dupuy, J. Claudon, J. M. Gérard, A. Auffèves, G. Nogues, S. Seidelin, J. P. Poizat, O. Arcizet, and M. Richard, Nat. Nanotechnol. **9**, 106 (2014).
- [35] C. A. Muschik, S. Moulieras, A. Bachtold, F. H. L. Koppens, M. Lewenstein, and D. E. Chang, Phys. Rev. Lett. **112**, 223601 (2014).
- [36] D. E. Liu and H. U. Baranger, Phys. Rev. B **84**, 201308(R) (2011).
- [37] K. Flensberg, Phys. Rev. Lett. **106**, 090503 (2011).
- [38] M. Leijnse and K. Flensberg, Phys. Rev. B **84**, 140501(R) (2011).
- [39] Y. S. Cao, P. Y. Wang, G. Xiong, M. Gong, and X. Q. Li, Phys. Rev. B **86**, 115311 (2012).
- [40] J. Li, T. Yu, H. Q. Lin, and J. Q. You, Sci. Rep. **4**, 4930 (2014).
- [41] X. D. Xu, B. Sun, P. R. Berman, D. G. Steel, A. S. Bracker, D. Gammon, and L. J. Sham,

- Science **317**, 929 (2007).
- [42] A. Zrenner, E. Beham, S. Stuffer, F. Findeis, M. Bichler, and G. Abstreiter, Nature **418**, 612 (2002).
 - [43] S. Stuffer, P. Ester, A. Zrenner, and M. Bichler, Phys. Rev. B **72**, 121301 (2005).
 - [44] K. F. Graff, *Wave Motion in Elastic Solids Dover* (New York, 1991).
 - [45] A. Ridolfo, O. Di Stefano, N. Fina, R. S. Saija, S. Savasta, Phys. Rev. Lett. **105**, 263601 (2010).
 - [46] R. W. Boyd, *Nonlinear Optics* (Academic, San Diego, Cal, 1992).
 - [47] H. J. Chen and K. D. Zhu, Sci. Rep. **5**, 13518 (2015).
 - [48] C. W. Gardiner and P. Zoller, *Quantum noise* (Berlin, Springer, 2000).
 - [49] J. J. Li and K. D. Zhu, Phys. Rep, **525**, 223 (2013).
 - [50] H. J. Chen and K. D. Zhu, RSC Adv. **4**, 47587 (2014).
 - [51] M. Fleischhauer, A. Imamoglu, and J. P. Marangos, Rev. Mod. Phys. **77**, 633 (2005).

Figure Captions

FIG.1 Sketch of the proposed setup for optically detecting Majorana fermions (MFs). (a) The energy-level diagram of a QD coupled to MFs and NR, which includes two kinds coupling, i.e. the QD-MF coupling (the dotted frame) and the QD-NR coupling (the dashed frame). (b) The iron chains on the superconducting Pb surface, and a pair of MFs appear in the ends of the iron chains. The nearby MF is coupled to (c) a QD embedded in a nanomechanical resonator (NR) with optical pump-probe technology.

FIG.2 The absorption (the blue curve) and dispersion (the green curve) spectra of probe field as a function of the probe detuning Δ_{pr} under different conditions. (a) Without considering any coupling, i.e., $g = 0$ and $\beta = 0$. (b) The QD-NR coupling strength is $g = 0.06$ and $\beta = 0$. (c) The QD-MF coupling strength is $\beta = 0.05$ GHz and $g = 0$. (d) Considering both the QD-NR coupling and QD-MF coupling, i.e., $g = 0.06$ and $\beta = 0.05$ GHz. The parameters used are $\Gamma_1 = 0.3$ GHz, $\Gamma_2 = 0.15$ GHz, $\gamma_m = 40$ kHz, $\omega_n = 1.2$ GHz, $\kappa_M = 0.1$ MHz, $\Omega_{pu}^2 = 0.005(\text{GHz})^2$, $\Delta_M = -0.5$ GHz, and $\Delta_{pu} = 0$.

FIG.3 (a) and (b) show the probe absorption (the blue curve) and dispersion (the green curve) spectra with QD-MF coupling strengths $\beta = 0.05$ GHz under $\epsilon_M \neq 0$ and $\epsilon_M = 0$, respectively. (c) The probe absorption spectrum under $\epsilon_M \neq 0$ (the green curve) and $\epsilon_M = 0$ (the blue curve), respectively. (d) The linear relationship between the distance of peak splitting and the coupling strength of QD-MF β . The other parameters used are the same as in Fig.2.

FIG.4 (a) The probe absorption spectrum as a function of the probe detuning Δ_{pr} with considering (the blue curve, $\beta = 0.1$ GHz) and without considering (the green curve, $\beta = 0$) the QD-MF coupling under the QD-NR coupling strength $g = 0.06$. (b) The exciton resonance spectrum as a function of Δ_{pr} with $g = 0$ and $g = 0.06$ at the QD-MF coupling strength $\beta = 0.1$ GHz. $\Delta_M = -1.2$ GHz, $\Delta_{pu} = 0.05$ GHz, $\Omega_{pu}^2 = 0.01(\text{GHz})^2$, The other parameters used are the same as Fig.2.

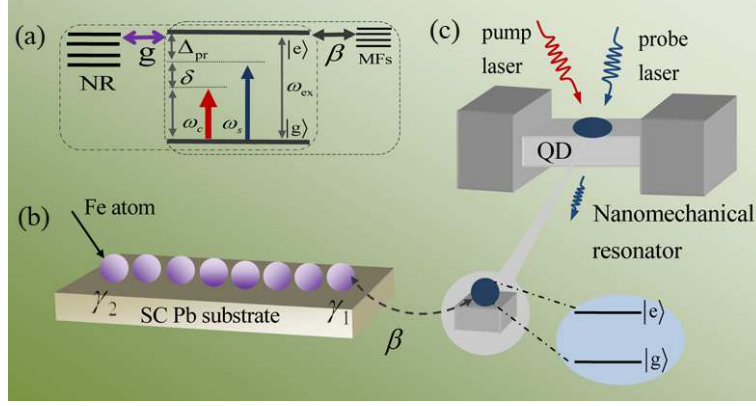


FIG. 1: Sketch of the proposed setup for optically detecting Majorana fermions (MFs). (a) The energy-level diagram of a QD coupled to MFs and NR, which includes two kinds coupling, i.e. the QD-MF coupling (the dotted frame) and the QD-NR coupling (the dashed frame). (b) The iron chains on the superconducting Pb surface, and a pair of MFs appear in the ends of the iron chains. The nearby MF is coupled to (c) a QD embedded in a nanomechanical resonator (NR) with optical pump-probe technology.

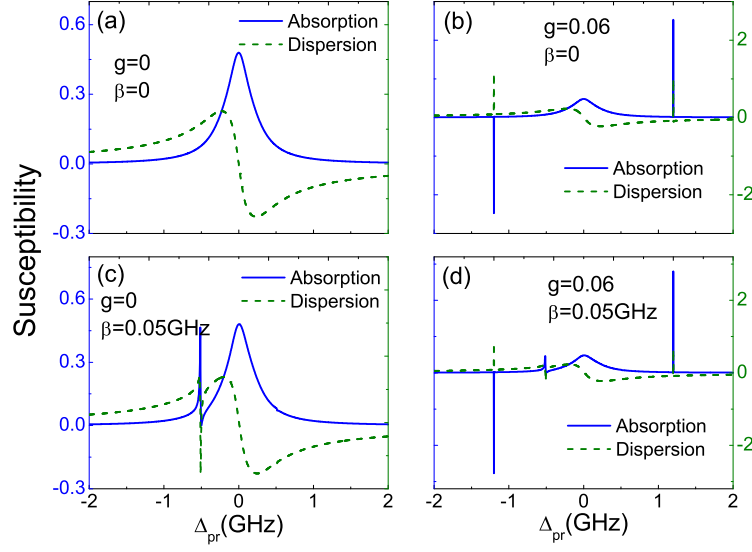


FIG. 2: The absorption (the blue curve) and dispersion (the green curve) spectra of probe field as a function of the probe detuning Δ_{pr} under different conditions. (a) Without considering any coupling, i.e., $g = 0$ and $\beta = 0$. (b) The QD-NR coupling strength is $g = 0.06$ and $\beta = 0$. (c) The QD-MF coupling strength is $\beta = 0.05$ GHz and $g = 0$. (d) Considering both the QD-NR coupling and QD-MF coupling, i.e., $g = 0.06$ and $\beta = 0.05$ GHz. The parameters used are $\Gamma_1 = 0.3$ GHz, $\Gamma_2 = 0.15$ GHz, $\gamma_m = 40$ kHz, $\omega_n = 1.2$ GHz, $\kappa_M = 0.1$ MHz, $\Omega_{pu}^2 = 0.005(\text{GHz})^2$, $\Delta_M = -0.5$ GHz, and $\Delta_{pu} = 0$.

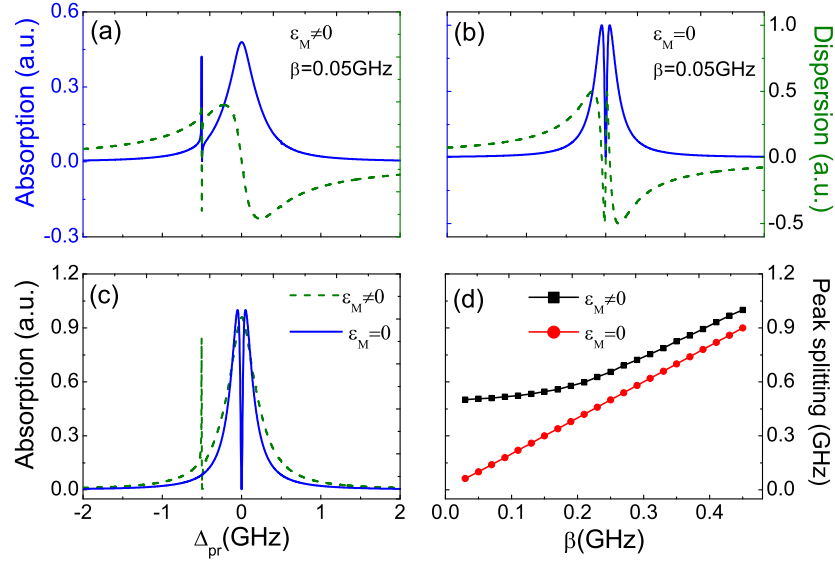


FIG. 3: (a) and (b) show the probe absorption (the blue curve) and dispersion (the green curve) spectra with QD-MF coupling strengths $\beta = 0.05$ GHz under $\epsilon_M \neq 0$ and $\epsilon_M = 0$, respectively. (c) The probe absorption spectrum under $\epsilon_M \neq 0$ (the green curve) and $\epsilon_M = 0$ (the blue curve), respectively. (d) The linear relationship between the distance of peak splitting and the coupling strength of QD-MF β . The other parameters used are the same as in Fig.2.

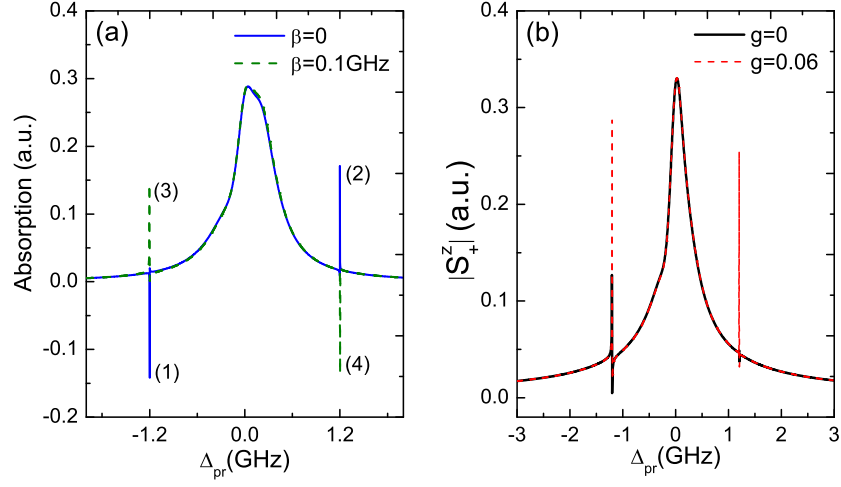


FIG. 4: (a) The probe absorption spectrum as a function of the probe detuning Δ_{pr} with considering (the blue curve, $\beta = 0.1$ GHz) and without considering (the green curve, $\beta = 0$) the QD-MF coupling under the QD-NR coupling strength $g = 0.06$. (b) The exciton resonance spectrum as a function of Δ_{pr} with $g = 0$ and $g = 0.06$ at the QD-MF coupling strength $\beta = 0.1$ GHz. $\Delta_M = -1.2$ GHz, $\Delta_{pu} = 0.05$ GHz, $\Omega_{pu}^2 = 0.01(\text{GHz})^2$, The other parameters used are the same as Fig.2.